THE SEASONAL VARIATION OF NIGHT-TIME SODIUM LAYER AT 33°N (II): ERROR ANALYSIS AND RESULTS FROM 1981 TO 1984

Michihiro UCHIUMI, Motokazu HIRONO and Motowo FUJIWARA

Department of Physics, Faculty of Science, Kyushu University, 10-1, Hakozaki 6-chome, Higashi-ku, Fukuoka 812

Abstract: Measurements of the night-time mesospheric sodium layer have been performed since 1977, using a dye lidar at Fukuoka (33.4°N, 130.2°E). The results obtained since 1981 are presented in this paper. The experimental setup and error analysis are also presented. A simple and sharp maximum in winter such as observed at other lidar stations in the northern hemisphere (51°N, 44°N, and 40°N) could not be found at Fukuoka. However, the monthly averaged abundance shows a variation by a factor of 3 (1981 and 1983). The abundance increased on the night during the Perseids γ meteor shower in 1978, 1979, 1981 and 1983 when the weather conditions did not preclude the observation of the sodium layer.

1. Introduction

Several workers have observed seasonal features of the upper atmospheric sodium layer by lidar (GIBSON and SANDFORD, 1971; MEGIE and BLAMONT, 1977; SIMONICH *et al.*, 1979; CERNY and SECHRIST, 1980). It is well known that the sodium density increases and the peak of the layer lowers slightly during winter at middle and high latitudes (HUNTEN, 1967).

Measurements of the night-time sodium layer have been performed intermittently since October 1977, using a dye lidar at Fukuoka (22.4°N, 130.4°E). The observations often reveal downward movements of a wavelike structure of the layer, but sometimes they do not show any vertical motion. The observational results about the variation throughout a night were already described (UCHIUMI and HIRONO, 1982). The main purpose of this paper is to present the seasonal variation of the sodium layer measured since 1981 at Fukuoka.

2. Experimental Setup

2.1. Laser

The Kyushu lidar uses a flashlamp pumped dye laser turned to the sodium D_2 line (589.0 nm) as a transmitter. The parameters of the lidar system are presented in Table 1. The dye laser developed in 1977 has been described elsewhere (NAGASAWA *et al.*, 1980). Improvements of the dye laser were made in January 1981. Their detailed description is given by NAGASAWA (1983), so only their important features

Table 1. Performances of the lidar system.

Laser		Receiver	
Wave Length	589.0 nm	Area	0.19 m²
Energy	1.0 J/pulse	Field of view	10 mrad
Line width	10 pm	Band width	1.0 nm
Pulse width	2 μs FWHM	Counter gate	10 μs
Repetition rate	0.25 Hz		
Beam divergence	0.5 mrad		

will be given here. The flashlamp pumped dye laser has high energy with narrow spectral band-width by a forced oscillator system and flashlamps in the simmer mode. A forced oscillator type dye laser has a larger gain than a single pass amplifier. It is a two-stage device with similar driver and forced oscillator head. The driver oscillator head contains a dye cell paired with a flashlamp with a capacitor. The forced oscillator head contains a dye cell surrounded by two flashlamps with their own capacitors. The driver oscillator has an elliptical reflector and the forced oscillator has a bi-elliptical reflector. Dye cells and flashlamps are placed on focal axes of each two reflector. These lamps are continuously evacuated with a resulting air pressure of 1–2 Torr. The spectral narrowing and tuning to the sodium D_2 line are obtained by placing two tilted Fabry-Perot etalons inside the cavity. The laser band width is 0.2 nm with the first etalon and 0.1 nm with the second one. The flashlamps and dye cells are associated with cooling jackets. The dye concentration is 8.5×10^{-5} mol/l Rhodamine 6 G in ethanol for the amplifier, and 5.1×10^{-5} mol/l Rhodamine 6 G in ethanol and water for the driver. The simmer current is provided at about 10 mA by a–2.2 kV DC power supply. The enhanced output from the forced oscillator with simmer operating is about 1.4 times larger than the output without simmer operating for Rhodamine 6 G (at 589.0 nm), and about 2 times for Coumarin (at 460.0 nm).

2.2. Interferometer

Firstly, the coarse tuning is performed using a grating spectrometer to a precision of 50 pm and with a sodium arc lamp providing the D_1 and D_2 lines for reference. Secondly, a Fabry-Perot interferometer and a sodium vapor cell are used to finely tune the center frequency of the laser line to that of the sodium line. The Fabry-Perot interferometer has the total finesse of 29. The resolving power of the interferometer is 2 pm with 3 mm spacers. The laser line width is also measured by the interferometer with an accuracy of 2 pm as described in the following.

A small part of the laser beam is injected into the Fabry-Perot interferometer by a beam splitter, and passed through a focusing lens and then projected on a camera screen. If one views the sodium lamp emission through the Fabry-Perot interferometer and the lens, fringe pattern of sodium D_1 and D_2 line will be seen. After taking pictures of the fringe pattern of the laser, the recorded films are read by a microdensitometer. The radius r and width Δr of fringe ring are measured, and one can determine the laser line width as follows:

$$\Delta\lambda \cong \frac{r\Delta r}{f^2}\lambda,$$

where f denotes the focal length of the focusing lens and is 475.7 mm (at wavelength of 589.0 nm). As a consequence, the measurement yielded line widths of 10–20 pm. There were twofold gradual changes in the line width during the intermittent observation since 1977. This is attributed mainly to the development of laser (January 1981), optical damages of Fabry-Perot etalon mirrors in the laser cavity (January and November 1982) and the exchanges for new ones (August 1982 and July 1983). On the other hand, it is known that the D_{2a} and D_{2b} lines are located 1.98 pm away from each other. Since the D_{2a} and D_{2b} lines are definitely resolved by this Fabry-Perot interferometer, we can determine its resolving power to be at least better than 2 pm. Therefore, our laser line width is found correct to 10–20% by the measurements. In this way, even if there is a variation in the line width of more than 2 pm throughout the night, this effect can be taken into account in the calculations of the effective scattering cross section. There is, however, scarcely a variation in the line width of more than 2 pm during at least about 4 hours.

3. Calibrating Parameters

The method of data analysis that we used is due to CERNY and SECHRIST (1980) as already mentioned in the earlier paper (UCHIUMI *et al.*, 1985). There is a more accurate method developed recently by SIMONICH and CLEMESHA (1983). Resonance extinction has a small effect of lidar returns from the upper atmospheric sodium. CERNY and SECHRIST (1980) underestimated the attenuation of upward path. Thus, application of CERNY and SECHRIST's method to our laser line width overestimated the absolute density by about 3%. Nonetheless, as the analysis has almost been over, we present the results based on CERNY and SECHRIST's method in this paper.

Following CERNY and SECHRIST (1980), the scattering cross section for the sodium D_2 line is expressed as

$$\sigma(\nu,T)=\sigma_0\left\{\frac{20}{32}\exp\left[-\frac{(\nu-\nu_{Da})^2}{2\sigma_D{}^2}\right]+\frac{12}{32}\exp\left[-\frac{(\nu-\nu_{Db})^2}{2\sigma_D{}^2}\right]\right\}. \tag{1}$$

Here σ_0 is the peak scattering cross section for the combined line and has a value of

$$\sigma_0=\frac{1.66\times10^{-6}}{\Delta\nu_D}\ \mathrm{m}^2, \tag{2}$$

where $\Delta\nu_D$ (Hz) denotes a Doppler broadened line width. Of course, $\Delta\nu_D$ is a function of the square root of the sodium temperature. The terms ν_{Da} and ν_{Db} represent the center frequencies of the D_{2a} and D_{2b}, respectively. The variance of the two Gaussian expressions, σ_D, is defined as:

$$\sigma_D{}^2=\frac{\Delta\nu_D{}^2}{8\ln 2}. \tag{3}$$

The effective cross section σ_{eff} is given by

$$\sigma_{eff}=\int_0^\infty g(\nu)\,\sigma(\nu,T)\,\mathrm{d}\nu, \tag{4}$$

where the line shape of the laser, $g(\nu)$, is assumed to be represented by a Gaussian form. An expression relating the number of photon counts originating from a specific altitude range to the sodium density is given in the earlier paper (UCHIUMI *et al.*, 1985). Usually, the normalizing altitude Z_r=35.25 km is selected. The Rayleigh scattering cross section $\sigma_r(\pi)$ evaluated at 35.25 km will be the value used in this study:

$$\sigma_r(\pi)=4.75\times 10^{-31}\mathrm{m}^2. \tag{5}$$

The air molecule number density at the normalizing altitude is obtained from the atmospheric model (U. S. Standard Atmosphere, 1976) and is assumed:

$$\rho_r=1.69\times 10^{23}/\mathrm{m}^3 \text{ at } 35.25 \text{ km}. \tag{6}$$

4. Error Analysis

In this section, we describe error analysis that we did not mention in the earlier paper (UCHIUMI *et al.*, 1985). The error of the absolute sodium density is obtained based on this analysis as follows:

$$\frac{\Delta\rho_i}{\rho_i}=\left[\left(\frac{\Delta\rho_r}{\rho_r}\right)^2+\left(\frac{\Delta\sigma_{\mathrm{eff}}}{\sigma_{\mathrm{eff}}}\right)^2+\left(\frac{\Delta N_i}{N_i}\right)^2\right]^{1/2}. \tag{7}$$

4.1. Error due to atmospheric density

At 30°N latitude, and 36 km latitude, the atmospheric density varies by 5% with the maximum value in February and with the minimum in August (CIRA, 1965). The first term in the righthand side, therefore, is 5% according to the U. S. Standard Atmosphere (1976). The density and column abundance presented in this paper are underestimated about 5% in August and overestimated about 5% in February. In the meantime, we can obtain the atmospheric density at an altitude of about 35 km by extrapolating the pressure and temperature data of the radiosonde, which is launched by Fukuoka Meteorological Observatory twice a day at a distance of 7 km southwest of our station. At present, by means of this extrapolation, the atmospheric density error has been reduced to 2%. Nevertheless, in order to compare new data with old ones, the density is based on the model (U. S. Standard Atmosphere, 1976) throughout a year.

4.2. Error due to effective cross section

The effective cross section of resonant scattering is obtained by eq. (4). Since we assume a vertical uniformity of the mesospheric temperature of 200 K, the error of eq. (4) comes from the uncertainty of measuring the laser line width and of the mesospheric temperature. First, the temperature at 95 km altitude at 30° latitude is estimated to be 187 K (May)–205 K (October) (CIRA, 1975). And the temperature at 85 km altitude is 179 K (June and July)–195 K (October) at the same latitude. Even if the temperature departure from 200 K is as large as 30 K, the error of the effective cross section due to the change of Doppler line width is 0.11% for our laser line width such as 10 pm. Therefore, the error of the sodium density is 0.11% by using the equation in the earlier paper (UCHIUMI *et al.*, 1985). For a line width as large as 20 pm, the error of the density at 170 K is only 0.027%. Therefore, the assumption

of constant temperature gives negligible effects on the sodium density calibration. Second, the error in measuring the laser line width described in Section 2.2, is 10–20%. Therefore, the error of effective cross section is 10–20% by using eq. (4). It is, however, assumed that there was no variation in the laser center frequency from the position of the D_2 line to calculate this error. The validity of this assumption is discussed below briefly. Such a broad line width as 20 pm has a disadvantage in measuring the mesospheric sodium whose Doppler broadening amounts to only 2–3 pm, because of a large energy loss. However, even if the laser center frequency is drifted 2 pm away from the D_2 line center, it gives only 1% density uncertainty because the laser line width is extremely broader than the D_2 line.

4.3. Error due to photon counts

N_i is the photon counts in the i-th range bin. The bin count error is due mostly to shot noise and is around $10\pm 5\%$ at the peak height for one profile obtained from 100 laser shots. If about 2000 shots of laser pulses are accumulated, the error of the third term becomes about 3% at the peak height. Here, it should be noted that there are variations in the number of shots accumulated for each night, ranging between 1000–5000 shots.

Finally, substituting the values described in Sections 4.1, 4.2 and 4.3 into eq. (7), the error in the sodium density is calculated to be 19–25% for about 100 laser shots and 12–21% for about 2000 shots. In this way, it is known that uncertainty of the measurements of the laser line width prevents accurate determination of the absolute density of the mesospheric sodium, which are the cases at another lidar stations. It can, however, be said that relative density profiles through a night are sufficiently reliable.

5. Observational Results

Figure 1 shows the seasonal variation of sodium layer observed at Fukuoka.

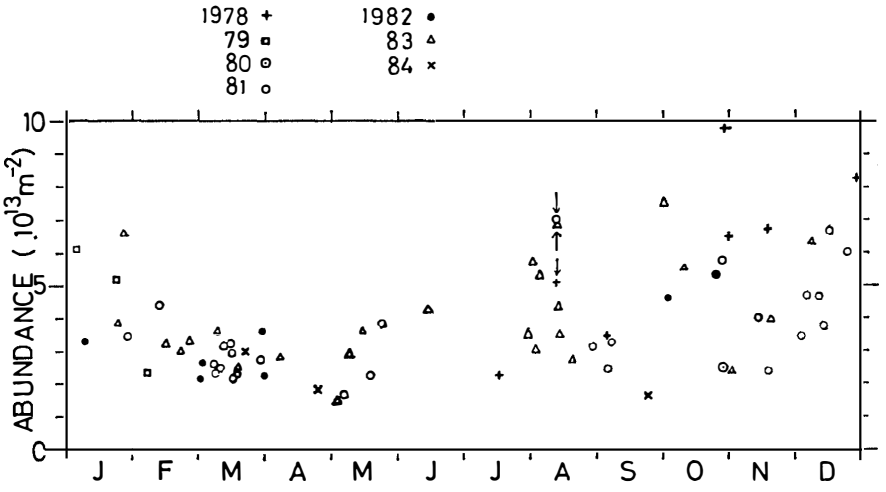

Fig. 1. Seasonal variation of Na total column abundance. The arrows correspond to anomalous values correlated with the Perseids γ meteor shower (see text).

It shows the mean column abundance of the sodium for each night on which observations were made. The arrows correspond to anomalous values correlated with the Perseids γ meteor shower. The years in which observations were made are indicated by symbols in the figure. The data in 1983 are calibrated again for this time and the results in the earlier paper (UCHIUMI *et al.*, 1985) are slightly corrected here. Figure 1 includes the results before December 1980 (after NAGASAWA) for reference. In this case, the density was calculated in relative unit since the uncertainty of the laser line width was large because of the degradation of resolving power of the Fabry-Perot interferometer. The results before 1980, therefore, are appropriately calibrated in absolute unit in this figure provided that the laser line width did not change with time. There may not be more than 50% difference in the absolute abundance between the results before and after December 1980.

The layer has a smaller abundance in spring, and a larger abundance in fall and winter. In March, the abundance is stable, and there is little day-to-day variation in the abundance. Moreover, there is little interannual variation in the abundance. On the other hand, there are large day-to-day and interannual variation in fall.

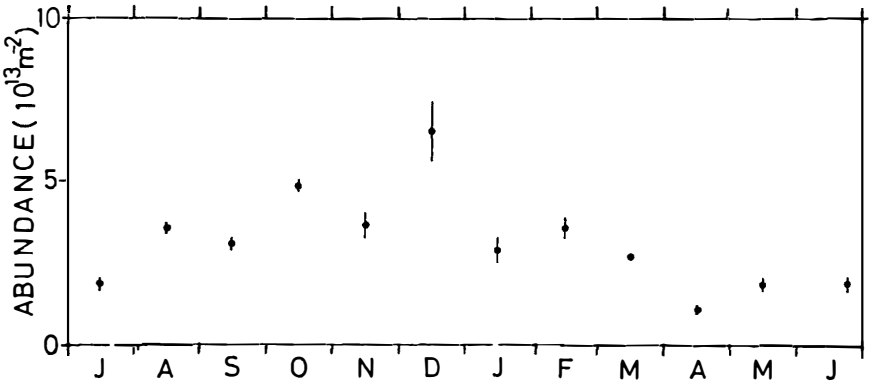

Fig. 2. Seasonal variation of the monthly mean of Na abundance averaged for two years, 1981 and 1983. The error bars indicate the error owing to the photon counts only.

Figure 2 shows the monthly averaged sodium abundance in 1981 and 1983. Since the stratospheric aerosol was dense and the observations are sparse in 1982, the data of 1982 are not included in the figure to increase the reliability of the figure. These values are calculated excluding anomalous values correlated with the Perseids γ meteor shower. And some noisy data of the observations in 1981 and 1983 are also excluded in the figure. The error bars are due to the photon counts only. The data in May, June and July are so sparse that the abundance are averaged over these three months. Figure 2 shows the seasonal variation by a factor of about 3 with maximum $6.5 \times 10^{13}/m^2$ in December, and with minimum $2 \times 10^{13}/m^2$ in April. Although the year-to-year variation is large in fall and winter as shown in Fig. 1, larger abundance in fall and winter and smaller abundance in spring are noticeable.

Figure 3 shows the variation of the altitude of the layer peak. The height resolution is 1.5 km. The average height is about 93 km. The peak is high in spring, and low in fall and winter.

The variation of the density of the peak is shown in Fig. 4. The average density

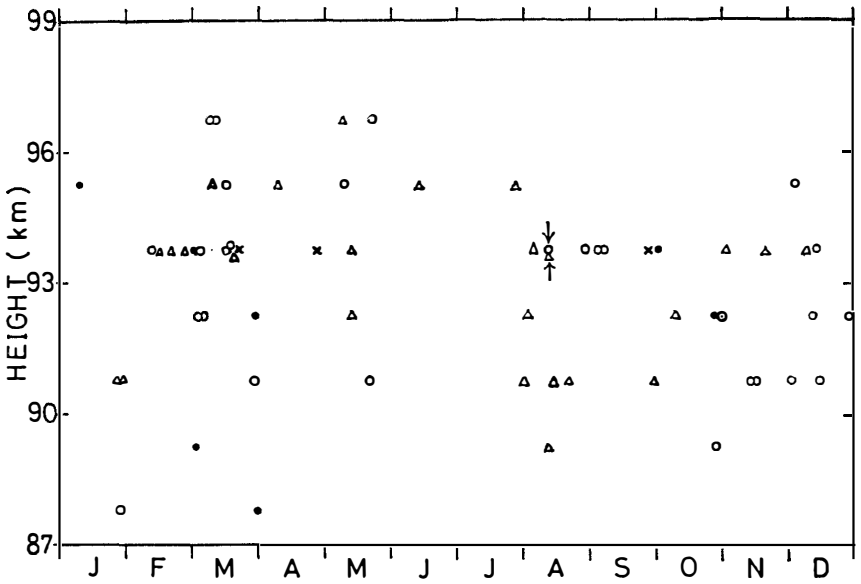

Fig. 3. Seasonal variation of the height of the maximum density. The height resolution is 1.5 km. The meaning of the symbols is given in Fig. 1.

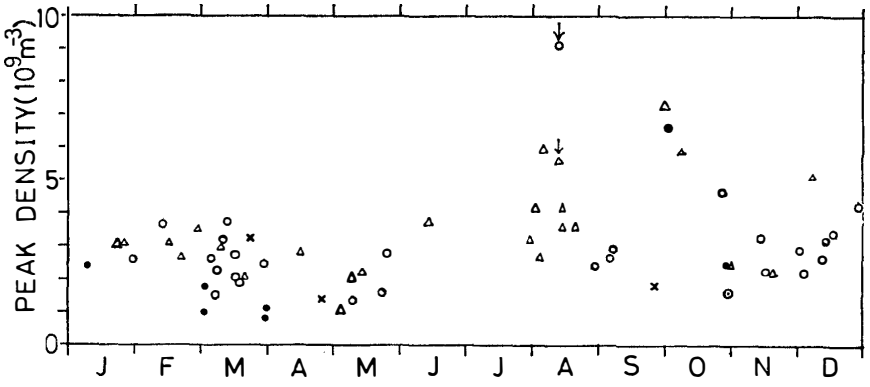

Fig. 4. Seasonal variation of the maximum density of the Na layer. See also the caption of Fig. 1.

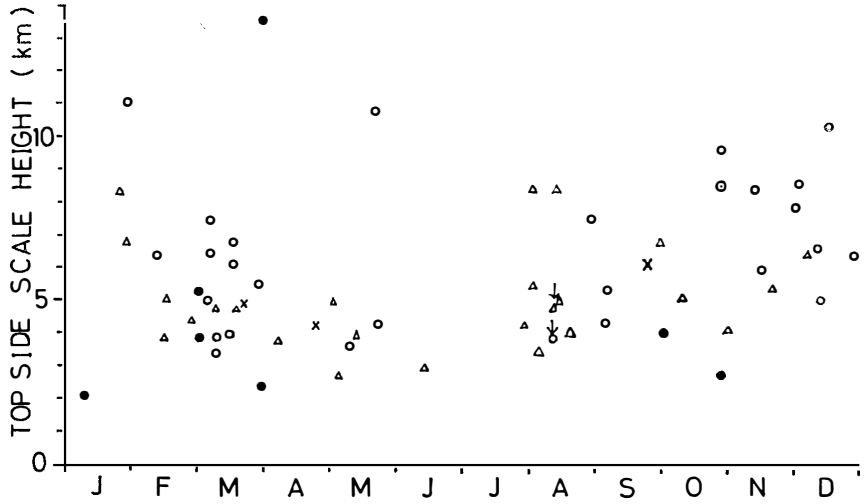

Fig. 5. Seasonal variation of the top-side scale height of the Na layer. See also the caption of Fig. 1.

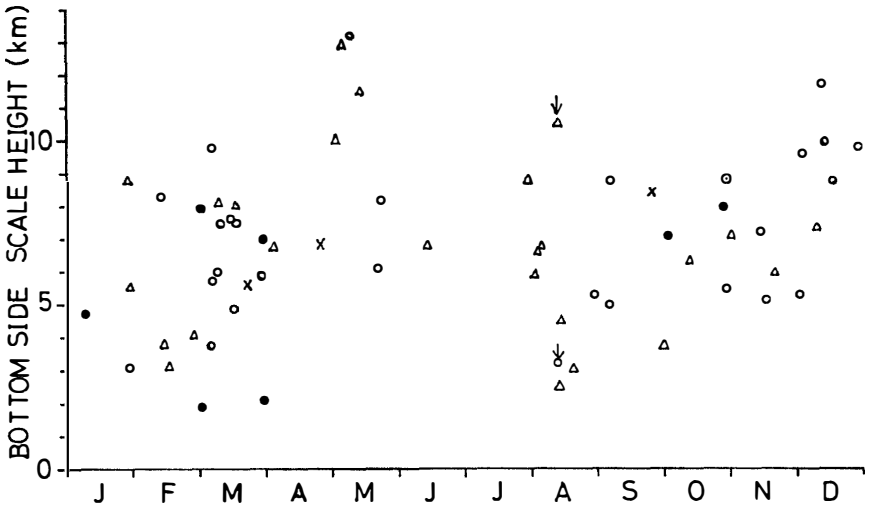

Fig. 6. Seasonal variation of the bottom-side scale height of the Na layer. See also the caption of Fig. 1.

is about $3 \times 10^9/m^3$. The peak density has maximum in fall. Figures 5 and 6 show the variation of top- and bottom-side scale height of the layer, respectively. The scale height of the sodium layer is defined as the height at which the density has fallen to e^{-1} of its peak value. The top-side scale height is large in fall rather than in spring. On the other hand, the bottom-side scale height is larger in early winter than in late winter.

In the meantime, the durations of our observations are 1–12 hours, and the average

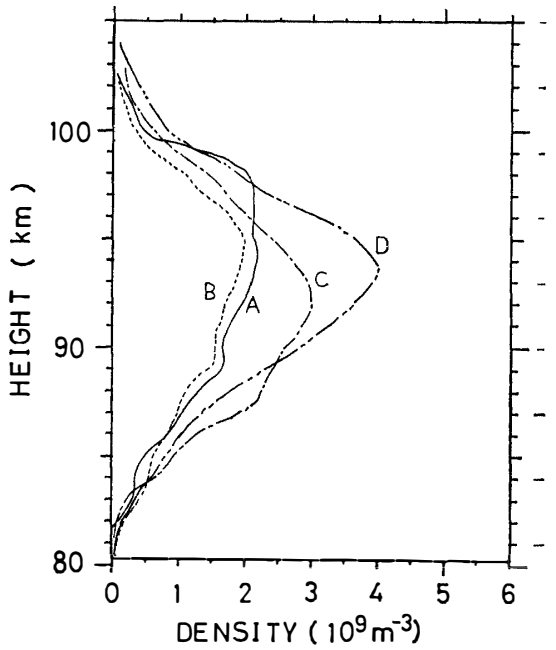

Fig. 7. Nocturnal variation of Na profiles averaged for three years from 1981 to 1983, including the Perseids γ meteor shower (see text). A: 1800–2059 JST, B: 2100–2359 JST, C: 0000–0259 JST, D: 0300–0600 JST.

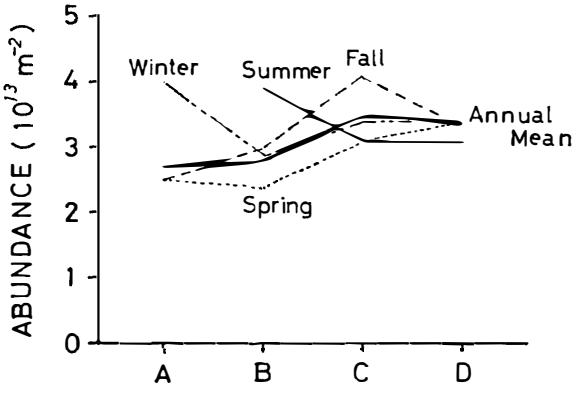

Fig. 8. Nocturnal variation of the Na abundance averaged for three years from 1981 to 1983, excluding the data correlated with the Perseids γ meteor showers. See also the caption of Fig. 7.

duration is about 4 hours. The start time of the observation is not specifically fixed. If the nocturnal variation of the sodium layer is large and durations of the observations are short, Fig. 1 may not show the seasonal variation only. Therefore, we need to discuss the nocturnal variation of the sodium layer. Figure 7 shows four sodium layer profiles which correspond to different time intervals of a night, averaged over the period from 1981 to 1983. A night is divided into four time intervals named A, B, C and D. A represents a time interval of three hours from 1800 to 2059 JST. B, C and D also represent the time interval of three hours indicated in the figure caption. Each vertical profile shown in Fig. 7 is derived from the photon counts integrated over the individual time interval of A, B, C and D, provided that the laser line width does not vary from 1981 to 1983. On individual night, the abundance does not always increase monotonically as the night progresses, and varies with time in various manners. It is found, however, that, on the average, the abundance of the layer increases as the night progresses. It should be noticed that these profiles also contained the data on the nights of the permanent meteor showers. The abundance of the layer tends to increase as the night progresses during the Perseids γ meteor shower. Some observations are concentrated around the night of permanent showers and they span almost the whole night. We simply summed up photon counts of data and calculated the density profiles shown in Fig. 7. Therefore, Fig. 7 shows particularly the features of the sodium at the time of permanent showers.

On the other hand, Fig. 8 shows the nighttime variation of the abundance excluding the data correlated with the Perseids γ meteor showers. The data of the time interval of A in summer are so sparse that the values are excluded in this figure. Such a tendency as seen in Fig. 7 almost vanishes in Fig. 8. Therefore, although Fig. 1 consists of the observations performed typically for only 4 hours, it is characterized by the seasonal variation rather than the nocturnal one.

6. Discussion and Conclusion

A simple and sharp maximum in winter such as observed at other lidar stations in the northern hemisphere (51°N, 44°N, 40°N) could not be found at Fukuoka. However, the monthly averaged abundance (1981 and 1983) shows the variation by a factor of 3 (Fig. 2). This ratio is slightly larger than the ratio of the recently developed model (JEGOU *et al.*, 1985).

As described in Section 5, the sodium abundance at Fukuoka increases in fall and winter, and decreases in spring. The sodium average peak height is high in spring and low in fall. The increment of the sodium abundance and lowering of the altitude of the layer occur simultaneously in fall. The lidar observations at Winkfield (51° N) (GIBSON and SANDFORD, 1971) also show similar tendency, but the increment of abundance is remarkable and the phase shifts: the increment and lowering of peak altitude occur simultaneously in December–January at 51°N.

According to the meteor radar observations at Kyoto (TSUDA *et al.*, private communication, 1985), meteor echoes increase in the morning and decrease in the evening. The temporal variation of the meteor echoes can be approximately expressed by a sinusoidal function. The variation of the peak height of the meteor echoes is ap-

proximately expressed by a normal distribution with a width of about 10 km and the peak at 95 km. The echoes increase from the middle of September to October, and decrease in summer. The average height is high in winter and low in summer, and the deviations from the average height are large in winter and small in summer. Therefore, the sodium results reported here differ from these meteor radar results. This is because, as well known, that the sodium abundance is likely to be affected by larger particles than radio meteor. However, the average peak height of the sodium layer obtained by our lidar and the peak height of the meteor echoes tend to coincide almost within 4 km in 1983.

Recently, JEGOU *et al.* (1985) suggested that the primary causes of the seasonal variations of the total abundance and of the peak altitude of the alkali layers are two fold:

(1) The seasonal change of the daytime duration at mesopause level (from 10 h during wintertime to 17 h during summertime at 44°N).

(2) The seasonal change of both atmospheric temperature and wind patterns.

The model consists of neutral reactions of sodium and clustering reactions of the sodium ion. The ion clusters are affected by Lorentz force of geomagnetic field and atmospheric wind. For ion clusters, the geomagnetic latitude is more important than the geographic latitude. (1) does not give a crucial effect on the seasonal variation of the sodium, particularly at low latitudes (JEGOU *et al.*, 1985). With respect to (2), mesospheric temperature was already suggested as a cause by other authors in the different manners (FIOCCO and VISCONTI, 1973: SIMONICHI *et al.*, 1979), which does not give reasonable explanation (JEGOU *et al.*, 1985). The cause due to the wind pattern is newly suggested in the model. JEGOU *et al.* suggested that the phase and the modulation of the seasonal variation are strongly dependent on the zonal wind pattern. Following their suggestion, we might infer that the interannual variation of the sodium in fall and winter (Fig. 1) is attributed to the interannual variation of the wind pattern, because there is a small interannual variation in temperature at our latitude. Experimental confirmation of this cause cannot be obtained due to the lack of observation of zonal wind near our site. The correlative study of the sodium layer with the mesospheric wind pattern may be necessary to make clear this point. With respect to the abundance and the peak height of the sodium layer, the model seems to give a reasonable explanation of the seasonal variation. However, the model does not give a realistic sodium profile particularly on the bottom side of the layer, probably, because the model (JEGOU *et al.*, 1985) includes only the following two reactions (Chapman reactions) for the neutral process:

$$Na + O_3 \rightarrow NaO + O_2, \tag{8}$$

$$NaO + O \rightarrow Na + O_2. \tag{9}$$

On the other hand, the seasonal variation of the temperature could solely play a crucial role in the seasonal variation of the sodium in the updated model (SWIDER, 1985) which consists of only neutral chemistry. SWIDER suggested that a chemical rate with inverse temperature dependencies enhances the seasonal variations of the sodium layer. The three-body reaction process,

$$Na + O_2 + M \rightarrow NaO_2 + M, \quad (10)$$

offers a reasonable explanation of the well-known seasonal effect observed for the mesospheric sodium layer, a higher content in winter. Because this has chemical rate constant with inverse temperature dependencies. However, the model does not explain a lower peak altitude of the layer in winter. Moreover, if the model (SWIDER, 1985) contains the ion clustering processes, it is not certain that the model gives a reasonable explanation of the sodium seasonal variation. Further study is still necessary to make clear this point.

The increment of the sodium abundance on the nights during the Perseids γ meteor shower is remarkable. Such a correlation has not been observed at low latitudes by lidar or photometric observations. Our observational results on the enhancement during the Perseids γ meteor shower will be described in detail in a later paper.

Acknowledgments

We would like to thank Mr. K. NISHIYAMA and Mr. H. AKIYOSHI for helping with some of the observations.

References

CERNY, T. and SECHRIST, C. F., Jr. (1980): Calibration of the Urbana lidar system. Aeronomy Report, 94, Aeron. Lab., Dep. Elec. Eng., Univ. Ill., Urbana-Champaign.

FIOCCO, G. and VISCONTI, G. (1973): On the seasonal variation of upper atmospheric sodium. J. Atmos. Terr. Phys., **35**, 165–171.

GIBSON, A. J. and SANDFORD, M. C. W. (1971): The seasonal variation of the night-time sodium layer. J. Atmos. Terr. Phys., **33**, 1675–1684.

HUNTEN, D. M. (1967): Spectroscopic studies of the twilight airglow. Space Sci. Rev., **6**, 493–573.

JEGOU, J. P., GRANIER, C., CHANIN, M. L. and MEGIE, G. (1985): General theory of the alkali metals present in the earth's upper atmosphere II. Seasonal and meridional variations. Ann. Geophys., **3**, 299–312.

MEGIE, G. and BLAMONT, J. E. (1977): Laser sounding of atmospheric sodium interpretation in terms of global atmospheric parameters. Planet. Space Sci., **25**, 1093–1109.

NAGASAWA, C. (1983): Development of dye laser radar and observation of the atmospheric sodium layer. Ph. D. thesis of Kyushu University.

NAGASAWA, C., HIRONO, M. and FUJIWARA, M. (1980): A reliable efficient forced oscillator dye laser to measure the upper atmospheric sodium layer. Jpn. J. Appl. Phys., **19**, 143–147.

SIMONICH, D. M. and CLEMESHA, B. R. (1983): Resonant extinction of lidar returns from the alkali metal layers in the upper atmosphere. Appl. Opt., **22**, 1387–1389.

SIMONICH, D. M., CLEMESHA, B. R. and KIRCHHOFF, V. W. J. H. (1979): The mesospheric sodium layer at 23°S; Nocturnal and seasonal variations. J. Geophys. Res., **84**, 1543–1550.

SWIDER, W. (1985): Enhanced seasonal variations for chemical rates with inverse temperature dependencies; Application to seasonal abundance of mesospheric sodium. Geophys. Res. Lett., **12**, 589–591.

UCHIUMI, M. and HIRONO, M. (1982): Shikiso raidâ ni yoru natoriumu sô no kansoku (The observation of the sodium layer by a dye lidar). Uchû Kansoku Shinpojium, Showa 57-nendo, ed. by D. Mori. Tokyo, Uchû Kagaku Kenkyûjo, 270–277.

UCHIUMI, M., HIRONO, M. and FUJIWARA, M. (1985): The seasonal variation of night-time sodium layer at 33°N. Mem. Natl Inst. Polar Res., Spec. Issue, **36**, 264–272.

(Received November 19, 1985; Revised manuscript received March 6, 1986)